

Discovery of Novel Potent and Highly Selective Glycogen Synthase Kinase-3 β (GSK3 β) Inhibitors for Alzheimer's Disease: Design, Synthesis, and Characterization of Pyrazines

Stefan Berg,^{*,†} Margareta Bergh,[†] Sven Hellberg,[†] Katharina Högdin,[†] Yvonne Lo-Alfredsson,[†] Peter Söderman,[†] Stefan von Berg,[†] Tatjana Weigelt,[†] Mats Ormö,[‡] Yafeng Xue,[‡] Julie Tucker,[§] Jan Neelissen,^{||} Eva Jerning,[⊥] Yvonne Nilsson,[#] and Ratan Bhat[▽]

[†]Department of Medicinal Chemistry, AstraZeneca R&D, Innovative Medicines CNS & Pain Södertälje, SE-151 85 Södertälje, Sweden

[‡]Discovery Sciences, AstraZeneca R&D Mölndal, SE-43183 Mölndal, Sweden

[§]Discovery Sciences, AstraZeneca R&D, Alderley Park, Macclesfield, Cheshire SK10 4TG, U.K.

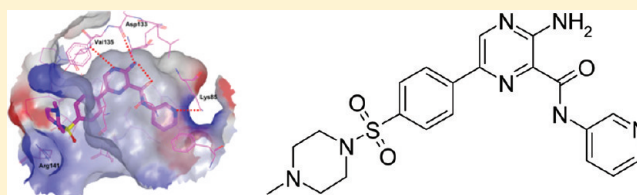
^{||}Department of DMPK, [⊥]Department of Neuroscience, AstraZeneca R&D, Innovative Medicines CNS & Pain Södertälje, SE-151 85 Södertälje, Sweden

[#]Department of Translational Sciences, AstraZeneca R&D Södertälje, SE-151 85 Södertälje, Sweden

[▽]Strategy, AstraZeneca R&D, Innovative Medicines CNS & Pain Södertälje, SE-151 85 Södertälje, Sweden

S Supporting Information

ABSTRACT: Glycogen synthase kinase-3 β , also called tau phosphorylating kinase, is a proline-directed serine/threonine kinase which was originally identified due to its role in glycogen metabolism. Active forms of GSK3 β localize to pretangle pathology including dystrophic neuritis and neurofibrillary tangles in Alzheimer's disease (AD) brain. By using a high throughput screening (HTS) approach to search for new chemical series and cocrystallization of key analogues to guide the optimization and synthesis of our pyrazine series, we have developed highly potent and selective inhibitors showing cellular efficacy and blood–brain barrier penetration. The inhibitors are suitable for in vivo efficacy testing and may serve as a new treatment strategy for Alzheimer's disease.



I INTRODUCTION

Alzheimer's disease¹ is a chronic neurodegenerative disorder affecting more than 25 million people worldwide. The disease is characterized by progressive cognitive decline such as loss of memory and orientation capability. Two major pathological hallmarks are observed in the AD brain. These are extracellular amyloid deposits,¹ consisting primarily of β -amyloid which is produced by proteolytic cleavage of the amyloid precursor protein, and intracellular neurofibrillary tangles,² primarily composed of hyperphosphorylated tau protein.

Glycogen synthase kinase-3 β , also called tau phosphorylating kinase, is a proline-directed serine/threonine kinase which was originally identified due to its role in glycogen metabolism. GSK3 β is abundant in the brain where it is localized primarily in neurons. GSK3 β phosphorylates tau, a microtubule associated protein, at sites which are abnormally hyperphosphorylated in AD. This leads to detachment of tau from the microtubules. The detached tau protein accumulates and aggregates in the somatosensory compartment of neurons, leading to the formation of paired helical filaments and subsequently neurofibrillary tangles and neuronal death.

Increased levels of total GSK3 β have not been consistently observed in AD brain, however, active forms of GSK3 β localize to pretangle pathology³ including dystrophic neuritis and neurofibrillary tangles (NFT) in AD brain. Neurons undergoing granulovascular degeneration⁴ also contain active GSK3 β . A spatial and temporal pattern of increased GSK3 β expression coinciding with the progression of NFT and neurodegeneration has also been observed. Taken together, these studies suggest that there is an increase in the active form of GSK3 β in degenerating neurons and pretangles. In preclinical studies, abnormal increased activity of GSK3 β has been shown to be associated with a multitude of adverse events linked to microtubule dysfunction, neuritic dystrophy and cytoskeletal damage, cognitive deficits, and amyloid production.⁵ Overexpression of GSK3 β in the brain of conditional transgenic mice resulted in tau hyperphosphorylation and somatodendritic localization of tau.⁶ Given the significant role of GSK3 β in a variety of

Special Issue: Alzheimer's Disease

Received: December 21, 2011

Published: April 10, 2012

effects linked to mechanism in AD and other central nervous system (CNS) disorders, GSK3 β inhibition using small-molecule inhibitors for treating particular disease states will be worth testing in the clinic.

Many research groups⁷ have reported diverse GSK3 β inhibitors over the last 10 years, but few have been potent and selective. Paullones were an early compound class where compound **1** (Figure 1, alsterpaullone^{8,9}) was shown to act as

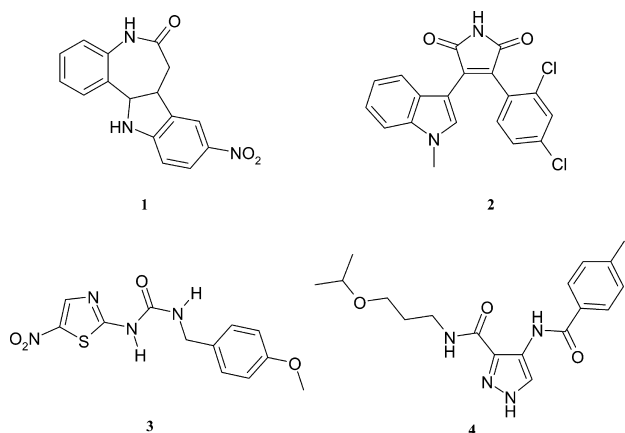


Figure 1. Reported GSK3 inhibitors.

an adenosine triphosphate (ATP) competitive GSK3 β inhibitor, however, compound **1** was also found to inhibit cyclin dependent kinase 2 (CDK2), a kinase with close homology within the ATP binding pocket. Another early cluster of compounds are the maleimide analogues where compound **2** (SB-216763¹⁰) from SmithKline Beecham represents one of the first potent GSK3 β inhibitors reported, inhibiting GSK3 β at an IC₅₀ of 9 nM. We reported in 2003 the crystal structure of the highly selective ATP competitive GSK3 β inhibitor **3** (AR-A014418¹¹) with an IC₅₀ of 104 nM.

More recently, Takeda Pharmaceuticals¹² has shown efficacy in a transgenic mouse model with the GSK3 β inhibitor **4** (6-methyl-*N*-[3-[[3-(1-methylethoxy)propyl]carbamoyl]-1*H*-pyrazol-4-yl]pyridine-3-carboxamide), suggesting that a GSK3 β inhibitor can prevent tau pathology in the brain.

In this report, we describe the discovery, characterization, and structure–activity relationship of a novel series of pyrazine analogues as potent GSK3 β inhibitors. We have used cocrystallization of key pyrazine analogues to guide the synthesis toward highly selective inhibitors which may serve as a new treatment strategy for Alzheimer's disease.

CHEMISTRY

By using a high throughput screening approach to search for new chemical series for the GSK3 β therapeutic target, we found several chemically diverse series showing moderate to high potency (nM– μ M). These series were also found active after retesting in the primary assay (GSK3 β enzyme).

One of the series, the pyrazines, initially showed good biochemical and physicochemical properties, and this initial lead was used for further optimization. One of the early actives from the high throughput screening campaign was compound **5** (Figure 2) in the pyrazine series, a GSK3 β inhibitor which showed acceptable potency (41 nM) when the HTS solution was retested.

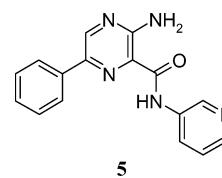


Figure 2. Compound **5**.

To investigate the structure–activity relationships and understand the selectivity vs CDK2 (a kinase with close homology within the ATP binding pocket) and other kinases, we synthesized a number of pyrazine analogues.

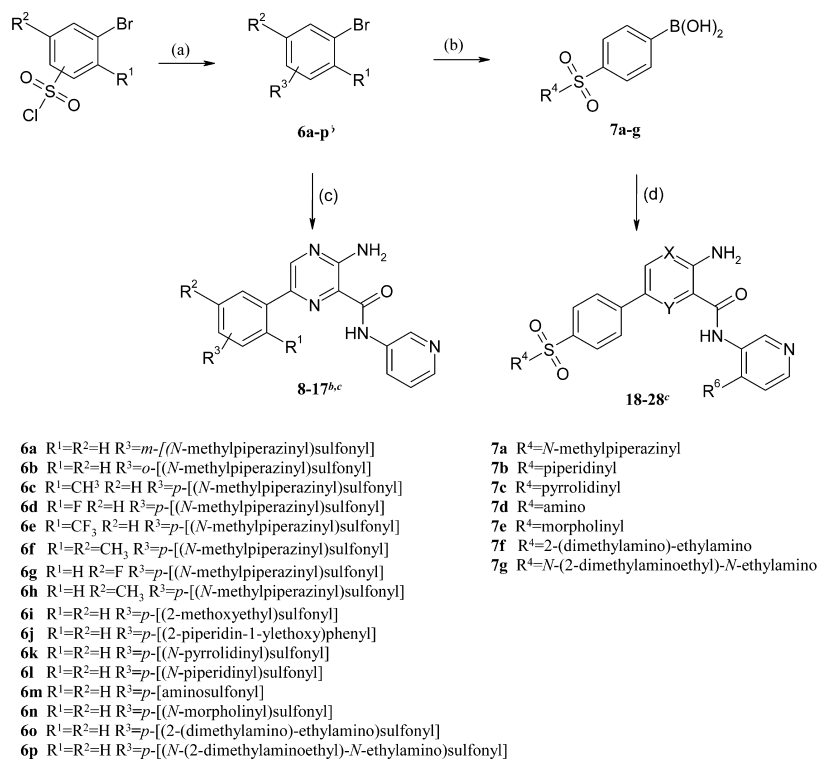
The synthesis of the kinase inhibitors is outlined in Schemes 1–7. The preparation of sulphonamides **8–28** is outlined in Scheme 1. Commercially available bromophenyl sulfonyl chlorides were treated with the appropriate amine to give the bromophenyl sulfonamides **6a,b,f–i,k–p**. The synthesis of bromides **6c–e** is outlined in Scheme 2. Compounds **8–17** were prepared in a one-pot reaction from the corresponding bromides **6a–j** via the in situ formed boronic acids and Suzuki reaction with the 6-bromopyrazines (**33**, **34a–b**, and **35a–b**, Scheme 3). The boronic acids **7a–g** were isolated with an acidic workup and subjected to Suzuki reactions to give compounds **18–28**. Data for compounds **8–28** are presented in Tables 1–3.

Bromides **6c–e** were synthesized as described in Scheme 2. The precursor anilines **30a–c** were prepared by treating the appropriate sulfonyl halide with 1-methylpiperazine. The sulfonyl halides were either commercially available (**29a**) or synthesized from either the sulfonic acid (**29b**) or the aniline (**29c**). The sulfonic acid **29b** was treated with thionyl chloride, and the aniline **29c** was subjected to direct sulfonylation using chlorosulfonic acid. The anilines **30a–c** were converted to the bromides **6c–e** via a Sandmeyer reaction by treating the formed diazonium salt with HBr and CuBr.

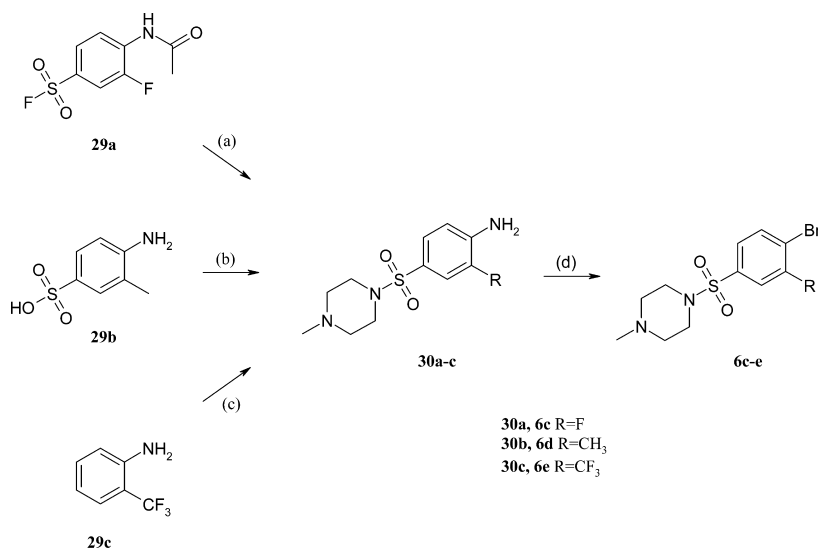
The 6-bromo-pyrazines (**33**, **34a–b**, and **35a–b**) required for the synthesis of compounds **8–28** were prepared from methyl 3-amino-6-bromo-pyrazine-2-carboxylate¹³ or the commercially available methyl 2-amino-5-bromobenzoate or methyl 2-amino-5-bromo-pyridine-3-carboxylate and the corresponding aniline (**32a–c**) as outlined in Scheme 3. Anilines (**32a–c**) were prepared by reductive amination of Boc-protected 3-aminopyridine-4-carbaldehyde with pyrrolidine or *N,N*-dimethylammonium hydrochloride using NaBH(OAc)₃ (**31a–b**), followed by deprotection of the Boc-group using trifluoroacetic acid (TFA) in dichloromethane.

Analogues **37–38** were prepared in a one-pot reaction (Scheme 4) first treating bromides **36a–b** with *n*-BuLi and B(O^{*i*}Pr)₃ to form the corresponding boronic acid followed by a Suzuki reaction with 3-amino-6-bromo-*N*-pyridin-3-ylpyrazine-2-carboxamide (**33**). The intermediate bromides (**36a–b**) were prepared by heating 4-bromobenzoic acid in refluxing thionyl chloride to give 4-bromobenzoyl chloride followed by treatment with the corresponding amine in DCM at 0 °C. Data for compounds **37–38** are presented in Table 1.

Compound **41** was prepared (Scheme 5) by diazotation of compound **18** followed by hydrolysis to give the pyrazinone **39**. This compound was treated with phosphoryl chloride to give the chloride **40**, which was reduced to **41** by heating with Pd(PPh₃)₄ and NaCO₂H in DMF at 100 °C. Data for compounds **41** are presented in Table 2.

Scheme 1^a

^aReagents: (a) NHRR', tetrahydrofuran (THF), dioxane, or dichloromethane (DCM); (b) *n*-BuLi, B(OⁱPr)₃, THF, -78 °C; (c) (1) *n*-BuLi, B(OⁱPr)₃, THF, -78 °C, (2) **33**, Pd(dppf)Cl₂, Na₂CO₃ (aq); (d) **33**, **34a–b**, or **35a–b**, Pd(dppf)Cl₂, Na₂CO₃ (aq), toluene/EtOH, 1,2-dimethoxymethane (DME), or THF. ^bPosition of R³ *o*-, *m*-, *p*- relative to bromine/pyrazine. ^cFor structures, see Tables 1–3.

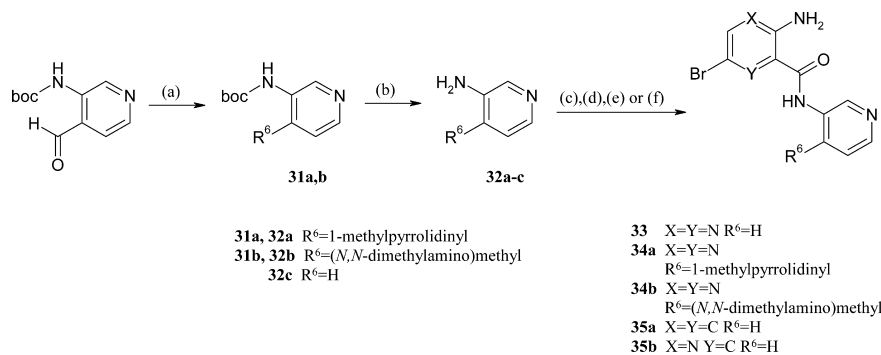
Scheme 2^a

^aReagents: (a) (1) 1-methylpiperazine, THF, rt to 60 °C, (2) HCl, 110 °C; (b) (1) SOCl₂, (2) 1-methylpiperazine THF/DCM; (c) (1) HSO₃Cl, 0–80 °C, (2) 1-methylpiperazine, THF; (d) NaNO₂, HBr/H₂O, and CuBr.

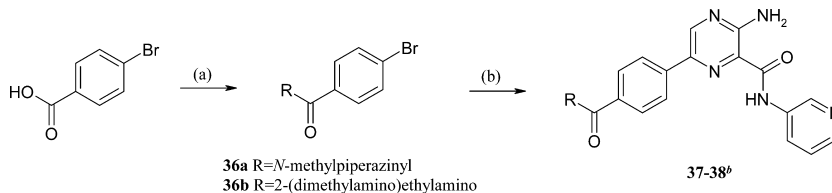
Compounds **44–46** were prepared (Scheme 6) by amidation of intermediate **43** with 2-methoxyaniline, 4-methoxyaniline, or 1,2,4-thiadiazol-5-amine in the presence of HOBt, TBTU, and DIPEA in DMF or using a mixture of DIPEA, HOBt, and bromo-tris-pyrrolidinophosphoniumhexafluorophosphate (Py-BroP) in DCM. Intermediate **43** was synthesized by a Suzuki reaction of 4-[(4-methylpiperazin-1-yl)sulfonyl]phenylboronic acid (**7a**) and methyl 3-amino-6-bromo-2-pyrazinecarboxylate

to give the methyl ester intermediate **42** that was subsequently hydrolyzed with LiOH in a mixture of THF and H₂O at 50 °C. Data for compounds **44–46** are presented in Table 3.

Compounds **49–51** were synthesized by a Suzuki coupling of 4-[(4-methylpiperazin-1-yl)sulfonyl]phenylboronic acid (**7a**) with bromides **48a–c** as outlined in Scheme 7. The intermediate bromides **48a–c** were prepared by amidation of 3-amino-6-bromo-pyrazine-2-carboxylic acid (**47**) with 3-methoxyaniline,

Scheme 3^a

^aReagents: (a) pyrrolidine and HOAc or dimethylammonium hydrochloride, NaBH(OAc)₃, DCM or 1,2-dichloroethane; (b) TFA, DCM; (c) 3-aminopyridine, methyl 3-amino-6-bromo-2-pyrazinecarboxylate, 1,8-diazabicyclo[5.4.0]undec-7-ene (DBU), 70 °C; (d) 3-amino-6-bromopyrazine-2-carboxylic acid or methyl 2-amino-5-bromo-pyridine-3-carboxylate, 1-hydroxybenzotriazole (HOBt), *O*-(benzotriazol-1-yl)-*N,N,N',N'*-tetramethyluronium tetrafluoroborate (TBTU), diisopropylethylamine (DIPEA), CH₃CN; (e) Et₃Al, methyl-2-amino-5-bromobenzoate, 3-aminopyridine, DCM reflux; (f) *N,N'*-diisopropylcarbodiimide (DIPC), HOBt, *N*-methylmorpholine-*N*-oxide (NMO), *N,N'*-dimethylformamide (DMF).

Scheme 4^a

^aReagents: (a) (1) SOCl₂, reflux, (2) 1-methylpiperazine or *N*¹,*N*¹,*N*²-trimethylethane-1,2-diamine, DCM, 0 °C; (b) (1) *n*-BuLi, B(O^{*i*}Pr)₃, THF, -78 °C, (2) 33, Pd(dppf)Cl₂, Na₂CO₃ (aq), THF, 70 °C. ^bFor structures see Table 1.

2-methoxyethylamine, or 3-methoxypropylamine using either a mixture of Et₃N, HOBt and TBTU in a mixture of DMF and CH₃CN or HOBt, 1-ethyl-3-(3-dimethylaminopropyl)-carbodiimide (EDCI) in CH₃CN. Data for compounds 49–51 are presented in Table 3.

RESULTS AND DISCUSSION

To investigate the chemical space defining GSK3β potency and kinase selectivity, three piperazinyl sulfonamide analogues 8, 9, and 18 were designed and synthesized (Table 1). Potency for the para-substituted sulfonamide analogue (18) increased 8-fold (*K*_i 4.9 nM) compared to compound 5, whereas potency for the meta (8) and ortho (9) isomers decreased to 79 and 300 nM, respectively. Many known GSK3β-inhibitors were also potent inhibitors of CDK2, a proline directed serine/threonine kinase showing high sequence similarity¹⁴ to GSK3β in the ATP binding site, hence selectivity versus CDK2 was routinely measured for all synthesized analogues in our GSK3β program. The three piperazine sulfonamides showed >100-fold selectivity versus CDK2. The solubility for 18 was found to be acceptable (35 μM) in the solubility assay likely due to protonation of the basic pyrazine nitrogen. We measured the permeability in Caco2 cells and obtained a *P*_{app} for 18 of 14 × 10⁻⁶ cm/s, indicating a putative good blood–brain barrier (BBB) penetration and bioavailability for this compound.

High resolution X-ray crystal structures of our lead pyrazine analogues bound to the GSK3β protein were generated. The structure confirmed the binding mode of the analogues in the ATP pocket of GSK3β. The X-ray crystal structure of compound 18 bound to GSK3β (Figure 3A) indicated that a pyrazine nitrogen and one of the adjacent anilino hydrogens

form hydrogen bonds to the backbone NH of Val135 and the backbone carbonyl of Asp133 in the ATP site.

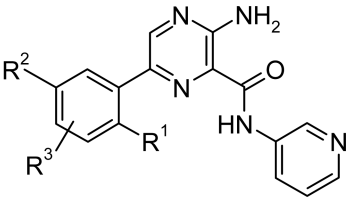
Furthermore, the carbonyl in the amide bond of compound 18 likely forms an internal hydrogen bond with the aniline group on the pyrazine ring, thus directing the pyridine ring toward the conserved Lys85 at the inner part of the ATP pocket. This would thus facilitate the formation of a hydrogen bond between the pyridine nitrogen and the terminal amino group of Lys85.

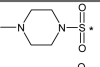
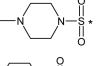
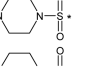
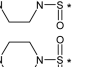
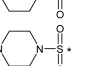
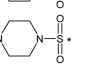
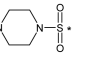
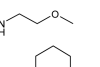
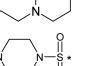
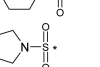
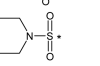
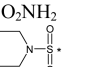
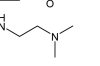
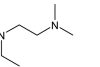
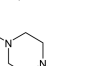
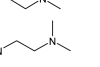
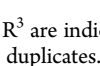
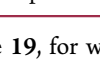
The 1-methylpiperazine sulfonamide is directed out toward the solvent (Figure 3B), adopting an upwards directed conformation. In this conformation, the sulfonamide functionality directly faces the guanidine group of Arg141. The sulfonamide group occupies a subpocket that is formed by the salt bridge between Glu137 and Arg141. The phenyl ring linking the sulfonamide to the pyrazinyl core is slightly twisted relative to the pyrazine ring (~20–30° anticlockwise).

Combining information from the potency data and the crystal structure, we chose to fix the position of the large solubilizing substituent, R³, in the para position of the phenyl ring.

Exchanging the 1-methylpiperazine for a piperidine (20) or a morpholine (22) increased the potency for GSK3β, resulting in a *K*_i of 0.4 and 0.67 nM, respectively. This increase in potency might be due to the removal of a potential repulsive interaction between the positively charged side chain of Arg141 and the basic pyrazine functionality in compound 18. This also resulted in a selectivity increase vs CDK2 of up to 550-fold for compound 20. When the ionizable nitrogen in the 6-membered aliphatic ring was replaced with a carbon atom (compound 20), the solubility dropped below 1 μM. This was also the case for

Table 1. GSK3 β Inhibition, CDK2 Selectivity, Solubility, and Caco2 Permeability Data for Pyrazines with Modifications in the Part of the Molecule Pointing out Towards the Solvent^a



Cpd#	R ¹	R ²	R ³	GSK3 β Ki (nM)	CDK2 Ki (nM)	Selectivity vs. CDK2 (fold)	Solubility (μ M)	Permeability Caco2 (10^{-6} cm/s)
8	H	H	meta 	74	24000	324	nd	nd
9	H	H	ortho 	300	42000	140	nd	nd
10	F	H		1.3	1000	770	11	11
11	CH ₃	H		0.46	1700	3700	90	24
12	CF ₃	H		1.1	2800	2540	202	37
13	CH ₃	CH ₃		1.5	>30000	>20000	242	38
14	H	F		9	1400	155	108	11
15	H	CH ₃		6.3	1100	174	nd	nd
16	H	H		2	94	48	54	20
17	H	H		18	5700	317	>2500	4.6
18	H	H		4.9	540	110	35	14
19	H	H		4.4	270	61	<1	nd
20	H	H		0.4	220	550	<1	nd
21	H	H	SO ₂ NH ₂	12	100	8.3	nd	<1
22	H	H		0.67	300	440	45	27
23	H	H		20	210	10	>2500	2.5
24	H	H		8.4	510	60	1400	11
37	H	H		3.1	1800	580	>2500	3.6
38	H	H		16	3900	244	>2500	1.9

^aPositions other than para substitution of R³ are indicated explicitly in the table by ortho or meta. * indicates point of attachment. Values are means of at least two experiments performed in duplicates. In Caco2 assay, $n = 1$. nd denotes no data.

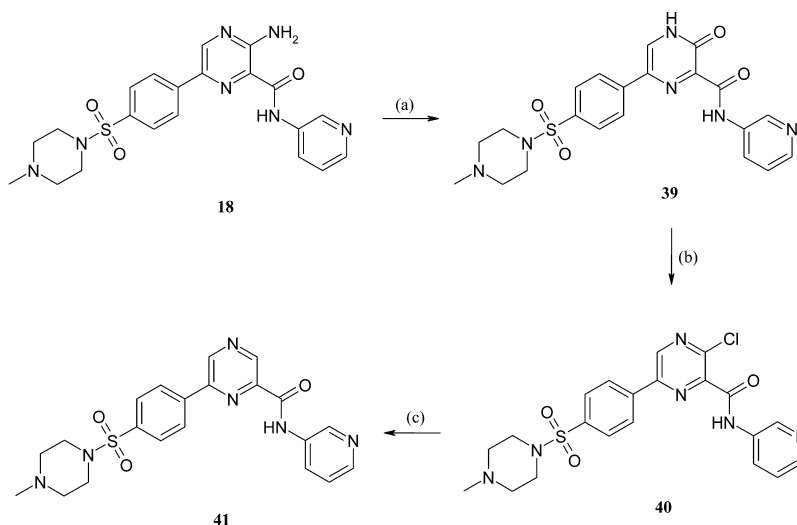
the 5-membered pyrrolidine analogue **19**, for which the potency toward GSK3 β and the selectivity against CDK2 were acceptable.

Introduction of a small R¹ substituent ortho to the pyrazine ring resulted in an increase in GSK3 β potency compared to **18**. Compounds **10**, **11**, and **12** gave a 4–10-fold increase in GSK3 β potency and a further increase in selectivity against CDK2 up to 3700-fold. The dimethyl analogue **13** showed the highest selectivity against CDK2 (>20000-fold) achieved within the pyrazine series. Solubility for this compound increased,

most likely due to a reduction in planarity while permeability likely increased due to an increase in lipophilicity.

To gain a deeper understanding of the selectivity against CDK2, X-ray crystal structures for compound **23** bound to GSK3 β and CDK2 were generated. See Figure 4A,B.

Comparison of the sequences and structures of the ATP site in CDK2 and GSK3 β (Figure 5) reveals a difference in amino acid sequence and protein structure at the phenyl subsite, especially in the areas around Pro136/Glu137/Thr138 in GSK3 β (His84/Gln85/Asp86 in CDK2) and Ile62 in GSK3 β (Ile10 in CDK2).

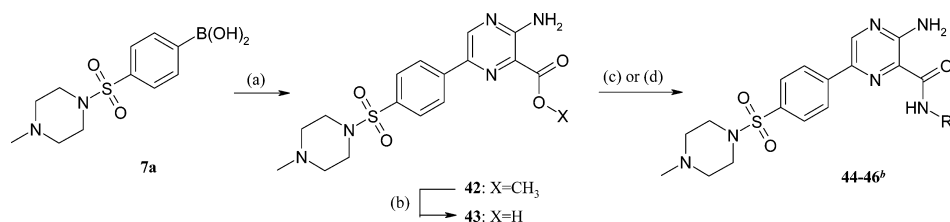
Scheme 5^a

^aReagents: (a) NaNO₂, H₃PO₂, H₂O, 50 °C; (b) POCl₃, 140 °C; (c) Pd(PPh₃)₄, NaCO₂H, DMF, 100 °C.

Table 2. GSK3 β Inhibition, CDK2 Selectivity, Solubility, and Caco2 Permeability Data for Sulfonamide Pyrazines with Core Modifications^a

compd	R ⁸	X	Y	GSK3 β K _i (nM)	CDK2 K _i (nM)	selectivity vs CDK2 (fold)	solubility (μ M)	permeability Caco2 (10 ⁻⁶ cm/s)
27	NH ₂	C	C	120	52000	433	50	nd
28	NH ₂	N	C	64	4900	77	4	nd
41	H	N	N	370	>30000	>81	119	25

^aValues are means of at least two experiments performed in duplicates. In Caco2 assay, $n = 1$. nd Denotes no data.

Scheme 6^a

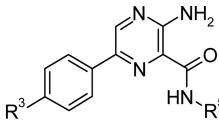
^aReagents: (a) methyl 3-amino-6-bromo-2-pyrazinecarboxylate, Pd(dppf)Cl₂, Na₂CO₃ (aq) or K₄PO₃ (aq), THF or dimethyl sulfoxide (DMSO)/H₂O or DME/H₂O, 50–160 °C; (b) LiOH, THF/H₂O, 50 °C; (c) 2-methoxyaniline or 4-methoxyaniline, HOBt, TBTU, DIPEA, DMF; (d) 1,2,4-thiadiazol-5-amine, DIPEA, HOBt, PyBroP, DCM. ^bFor structures see Table 3.

The presence of Pro136 in GSK3 β leads to a difference in main chain conformations, making this area of the pocket in GSK3 β significantly larger (in the vertical direction) than in CDK2 (areas indicated by yellow dashed circles in Figure 5). We observed from the X-ray structures that the phenyl ring of compound **23** is in a nonplanar arrangement with respect to the pyrazine ring (dihedral angle of +21 in GSK3 β and -13 in CDK2). Thus, we concluded that the selectivity for GSK3 β may be a result of the GSK3 β ATP site being able to leverage a nonplanar binding mode and a concomitant increase in three-dimensional bulk.

On the bases of the X-ray crystal structures, we hypothesized that compounds with R¹ substituents further accentuate the nonplanarity, leading to the observed increase in selectivity vs CDK2 (compounds **11–13** in Table 1). Compounds with a substituent in the R² position (**14** R² = F and **15** R² CH₃) resulted in potencies and selectivities comparable to compound **18**.

In an attempt to reduce the size of our analogues, the primary sulfonamide **21** was synthesized. This resulted both in a drop in potency (12 nM) and selectivity (8-fold). In addition, the permeability was reduced to below detection level, most likely due to the introduction of two additional hydrogen bond

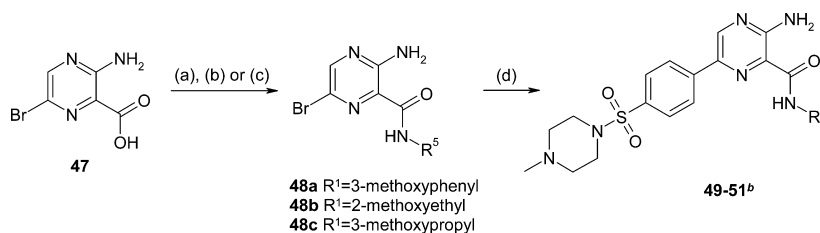
Table 3. Inhibition, Selectivity, Solubility, and Permeability Data for Sulfonamide Pyrazines with Modifications in the Part of the Molecule Pointing Towards the Conserved Salt Bridge^a



Cpd#	R ³	R ⁵	GSK3β Ki (nM)	CDK2 Ki (nM)	Selectivity vs. CDK2 (fold)	Solubility (μM)	Permeability Caco2 (10 ⁻⁶ cm/s)
25			0.22	130	591	46	2.3
26			0.48	56	117	<1	nd
44			12	1900	158	14	1.3
45			690	>30000	>43	nd	nd
46			0.99	43	44	12	18
49			74	>30000	>405	nd	nd
50			90	5800	64	147	nd
51			22	2800	127	126	14

^a* indicates point of attachment. Values are means ± standard error of the mean (SEM) of at least two experiments performed in duplicates. In Caco2 assay, *n* = 1. nd denotes no data.

Scheme 7^a



^aReagents: (a) 3-methoxyaniline, Et₃N, HOBt, TBTU, DMF/CH₃CN; (b) 2-methoxyethylamine or HOBt, EDCI, CH₃CN; (c) 3-methoxypropylamine, HOBt, TBTU, DIPEA, DMF; (d) [4-[(4-methyl-1-piperazinyl)sulfonyl]phenyl]boronic acid (7a), Pd(dppf)Cl₂, Na₂CO₃, THF/H₂O, MW 70 °C. ^bFor structures see Table 3.

donors. Introduction of an amino containing carbon chain on the sulfonamide (**23**) substantially increased solubility (>2500 μM). By introducing a second substituent on the sulfonamide (ethyl, **24**), the permeability was increased while retaining potency and solubility. Compound **16**, which lacks the solubilizing amino functionality, gave a lower solubility. The corresponding amide analogues showed comparable potency and selectivity profiles to the sulfonamides. Compounds **37** and **38** showed a potency of 3.1 and 16 nM and a 600- and 250-fold selectivity vs CDK2, respectively. Solubility was substantially higher for the amides compared to the sulfonamides, however, the permeability decreased for both compounds. Acceptable potency, selectivity, solubility, and permeability were also achieved with the aminoalkyl ether **17** (*K_i* 18 nM).

The chemical scope for the core pyrazine was also investigated. Compared to compound **18**, the corresponding pyridine analogue **28** showed a 12-fold drop in potency (Table 2). This might be due to a conformational effect caused by loss of the partial internal hydrogen bond between the pyrazine

nitrogen and the NH of the amide functionality. An alternative explanation could be that the replacement of nitrogen with carbon may have an electronic effect with an indirect impact on the hydrogen bonding strength to the hinge region. Removal of the second nitrogen resulted in the phenyl analogue **27** with an *K_i* of 120 nM, a 24-fold decrease compared to compound **18**. When the amino group on the pyrazine was removed, compound **41** R⁸ = H, the potency for GSK3β was reduced dramatically (*K_i* 370 nM). The solubility for the three compounds varied between 4 and 119 μM.

The modifications in compound **27** and **41** reduced the number of hydrogen bond interactions available to the backbone of the hinge region of GSK3β, and possibly also the hydrogen bonding strength, which explains the dramatic drop in potency for the two compounds.

Highly potent inhibitors were also found through the synthesis of the 4-substituted benzyl aminopyridines **25** (*K_i* 0.22 nM) and **26** (*K_i* 0.48), which show moderate to good selectivity vs

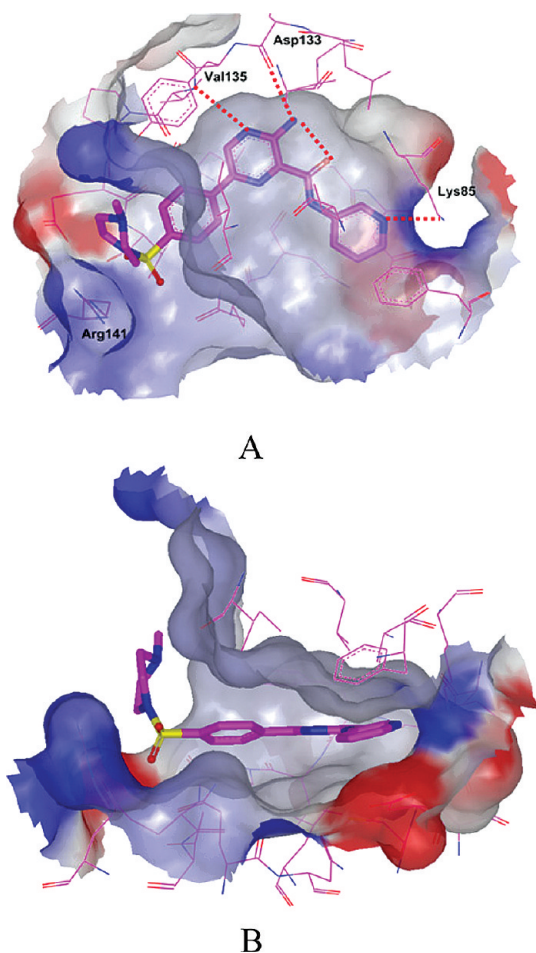


Figure 3. X-ray crystal structure of compound **18** in the GSK3 β ATP site. (A) Top view; (B) side view. Resolution 2.6 Å. Figures were prepared using VIDA 4.0.3 from OpenEye Scientific Software, 9 Bisbee Court, Suite D, Santa Fe, NM 87508.

CDK2 (Table 3). Although permeability was relatively low, the solubility was acceptable for **25**.

Figure 6A shows the X-ray crystal structure of the benzylpyrrolidine **25** in the ATP site of GSK3 β . The overall binding mode is the same as that observed for compound **18**,

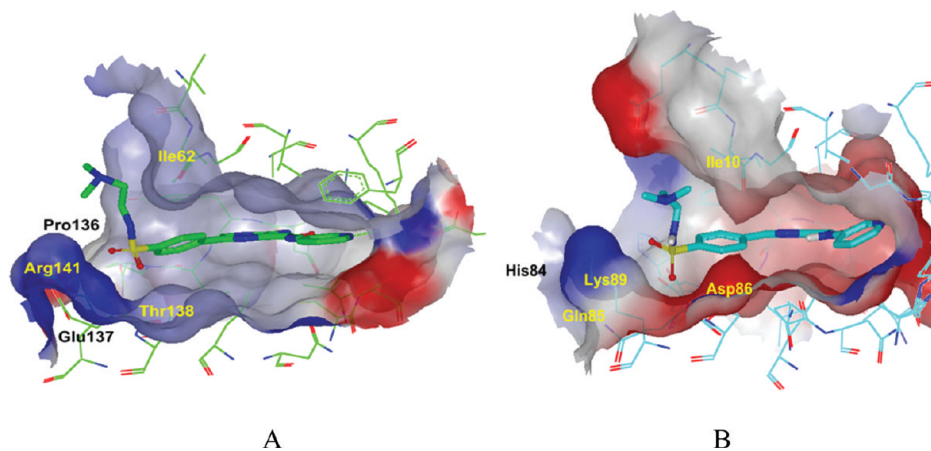


Figure 4. (A) X-ray crystal structure of compound **23** in the GSK3 β ATP site, resolution 2.5 Å. (B) X-ray crystal structure of compound **23** in the CDK2 ATP site, resolution 1.63 Å.

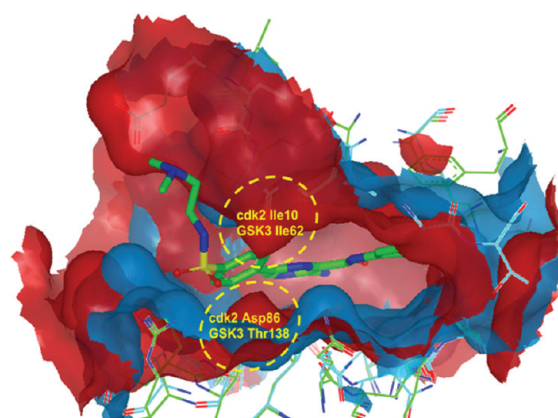


Figure 5. X-ray crystal structure of compound **23** in the GSK3 β ATP site (blue surface) aligned with CDK2 ATP site (red surface).

with the polar pyrrolidine ring extending toward and partially filling the ribose binding site, resulting in a 22-fold increase in potency compared to compound **18**. This site is occupied by a water molecule in the crystal structure of compound **18**. The presence of the pyrrolidine ring has also resulted in a slight upward movement of the phenyl ring and thus the attached sulfonamide and methylpiperazine moieties (~ 1 Å at the sulfur) and an increase in the twist between the pyrazine and the phenyl rings to about 40° (vs about 20° for compound **18**), resulting in a 580-fold CDK2 selectivity (Figure 6B). This change led to better van der Waals interaction to the side chain of Ile62 (part of the Gly-rich loop). Furthermore, the “space-filling” effect of the pyrrolidine ring in the ribose binding area (e.g., the van der Waals interaction to the glycine-rich loop) may also contribute to the increase in binding affinity compared to compound **18**. Potency was thus improved by interacting with the ribose site. The alignment of compound **18** and **25** in the ATP site of GSK3 β (Figure 6B) shows that, although the pyridine nitrogen is in the same position in both compounds, the solubilizing piperazine ring is shifted slightly up and out toward the solvent area for compound **25**.

To investigate whether the 3-pyridine ring could be replaced with a substituted phenyl ring, the ortho (**44**), meta (**49**), and para (**45**) methoxy isomers were synthesized.

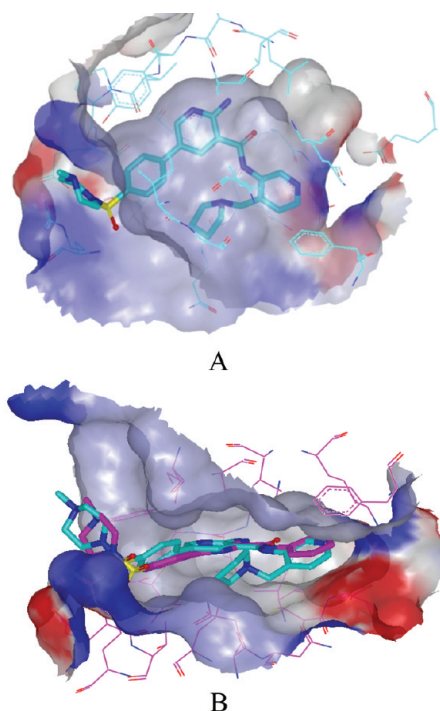


Figure 6. (A) X-ray crystal structure of compound **25** in the GSK3 β ATP site. Resolution 2.6 Å. (B) Alignment of compound **18** (pink) and **25** (blue) in the ATP site.

The ortho analogue, where the methoxy group likely extends toward the ribose binding site, showed the highest potency (12 nM) of the three analogues with 160-fold selectivity against CDK2, however, both the permeability and solubility were low. The meta and para analogues showed a 16- and 140-fold drop in potency compared to **18**. Thus the conclusion was that neither the meta nor the para methoxy could reach Lys85 and form a productive hydrogen bond.

The 5-membered heteroaromatic thiadiazole analogue **46** showed a high potency of 0.99 nM, 44-fold selectivity against CDK2, and good permeability. Finally, the corresponding methoxy substituted aliphatic amides were made. Potency and selectivity is observed to increase with the methoxy-carbon chain length. The 2-methoxyethyl analogue **50** is substantially less potent (90 nM) than the 3-methoxypropyl analogue **51** (22 nM).

Initial docking studies suggested that the alkoxy modification could replace the pyridine of compound **18**, with the alkoxy function extending sufficiently to be within hydrogen bond distance of Lys85. The observed potency for the alkoxy analogues appeared to support this docking hypothesis. However, subsequent X-ray crystal structures showed a different binding mode, leading us to reject our initial hypothesis. The methoxypropyl substituent (**51**) instead extends toward the ribose binding area of the GSK3 β ATP pocket (Figure 7A). The folded-back conformation of the methoxypropyl group resembles the pyrrolidine group in compound **25** (Figure 7B), i.e., “space-filling” the ribose pocket and also stabilizing the twist between the pyrazine and the phenyl rings of the ligand (similar twisting of $\sim 40^\circ$ is observed for both compound **25** and **51**). This interaction apparently compensates, at least partly, for loss of the hydrogen bond to Lys85 via the 3-pyridine in compound **18** and **25**.

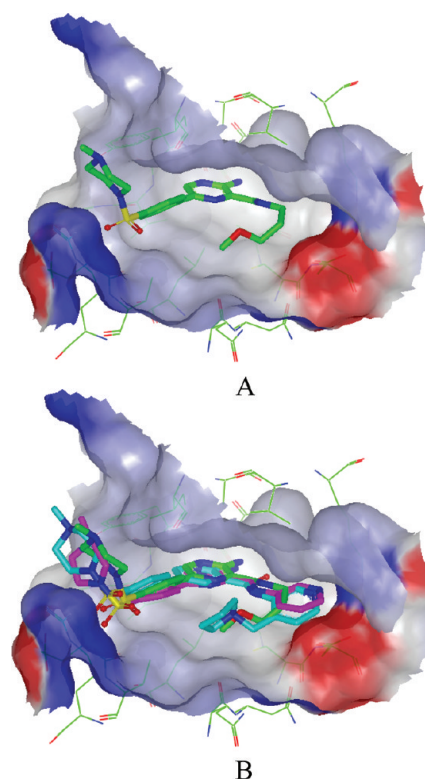
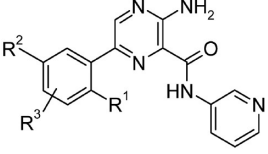


Figure 7. (A) X-ray crystal structure of compound **51** bound in the GSK3 β ATP site. Resolution 2.8 Å. (B) Superimposition of compound **18** (pink), **25** (blue), and **51** (green).

Inhibition of Tau Phosphorylation. To evaluate whether analogues from the pyrazine series inhibit GSK3 β -mediated tau phosphorylation in cells, 3T3 fibroblasts were engineered to stably express four-repeat tau protein. Transfected cells were treated with vehicle (0.1% Me₂SO) or with increasing concentrations (100 nM to 50 μ M) of compounds **11**, **12**, **14**, **16**, **18**, **19**, **22**, **23**, and **25** and harvested 4 h after treatment. The effect on tau phosphorylation in the presence or absence of serum was determined by Western blotting. Detection was carried out using a phosphospecific antibody, which detects an epitope on tau (Ser(P)-396), a site which is specifically phosphorylated by GSK3 β in cells. Total levels of tau in the samples were determined by stripping the blot and reprobing with a phosphorylation independent antibody to total tau protein (Tau5). The bands were quantified by densitometric analysis. The levels of Ser(P)-396 were not affected by changes in serum. Tested compounds inhibit tau phosphorylation in the transfected cells in a dose-dependent fashion, exhibiting IC₅₀s ranging from 5 to 87 nM, as shown in Table 4.

Pan-Kinase Selectivity. Compound **18** was evaluated for pan-kinase selectivity (10 μ M) at the University of Dundee. The compound shows a good overall selectivity versus 26 kinases (Figure 8). The CDK2 K_i was determined in-house and was shown to be 510 nM, corresponding to a 110 fold selectivity versus CDK2.

Blood–Brain Barrier Permeability. To investigate whether our compounds were suitable for in vivo testing of GSK3 β inhibition in the brain, compound **18** and its analogues **14**, **16**, and **22** were tested for blood–brain barrier permeability in a bovine endothelial cell assay.¹⁵ All four compounds showed a good permeability in this assay, indicating that a considerable total brain exposure can be expected when dosed in vivo (Table 5).

Table 4. Inhibition of Tau Phosphorylation in 3T3 Cells^a


Cpd#	R ¹	R ²	R ³	Tau inhibition IC ₅₀ (nM)
11	CH ₃	H		11
12	CH ₃	H		5
14	H	F		49
16	H	H		79
18	H	H		76
20	H	H		87
22	H	H		10
23	H	H		37
24	H	H		47

^a* indicates point of attachment. Values are means \pm SEM of at least two experiments performed in duplicates. nd denotes no data.

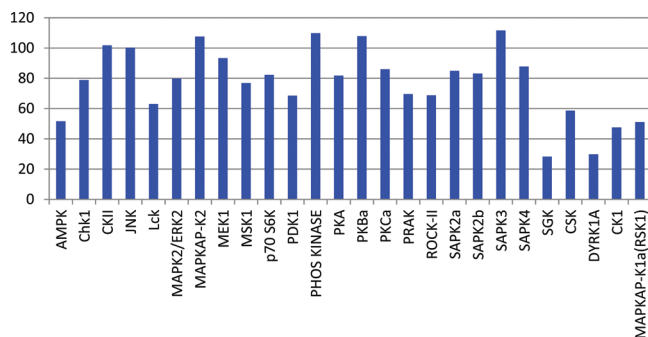


Figure 8. Kinase activity at 10 μ M. Effect of compound 18 on the activities of 26 protein kinases in vitro. Protein kinases were assayed in the presence of 10 μ M compound 18 or vehicle (DMSO). The enzymatic activity was measured in the presence of 0.1 mM ATP. Kinase activities are given as the mean of triplicate determinations. AMPK, AMP-activated protein kinase; Chk, checkpoint kinase; CKII, casein kinase-2; JNK, c-Jun N-terminal kinase; Lck, lymphocyte c-Src kinase; MAPK, mitogen-activated protein kinase; MAPKAPK-2, mitogen activated protein kinase-activated protein kinase-2; MEK1, mitogen-activated protein kinase/extracellular signal-regulated kinase-1; MSK1, mitogen- and stress-activated protein kinase-1; p70 S6K, p70 ribosomal protein S6 kinase; PDK1, 3-phosphoinositide-dependent protein kinase-1; PhosK, phosphorylase kinase; PKA, protein kinase A; PKBa, protein kinase B; PKCa, protein kinase C; PRAK, p38-regulated/activated kinase; ROCKII, Rho-dependent protein kinase II; SAPK2a, stress-activated protein kinase-2a; SAPK2b, stress-activated protein kinase-2b; SAPK3, stress-activated protein kinase-3; SAPK4, stress-activated protein kinase-4; SGK, serum- and glucocorticoid-induced kinase; CSK, carboxyl-terminal Src kinase; DYRK1A, dual-specificity tyrosine phosphorylation-regulated kinase; CK1, casein kinase-2; RSK1, ribosomal S6 kinase-1.

Table 5. Blood–Brain Barrier (BBB) Permeability Data in Bovine Endothelial Cells^a


Cpd#	R ¹	R ²	R ³	BBB permeability (10 ⁻³ cm/min)
14	H	F		3.9
16	H	H		12
18	H	H		15
22	H	H		23

^a* indicates point of attachment. $n = 1$.

CONCLUSIONS

Inhibition of tau kinases may have therapeutic effects on the progression of chronic degenerative diseases such as Alzheimer's and other tauopathies. In this report, we have described a new structural class of GSK3 β inhibitors. The pyrazine structural class has generated several highly potent and selective inhibitors showing good solubility and permeability in both the Caco2 and BBB assays and thus predicting good bioavailability and brain penetration. Several pyrazine analogues are suitable for testing of inhibition of tau phosphorylation in the brain, and the inhibitors have potential as novel therapeutic agents for the treatment of neurodegenerative diseases.

EXPERIMENTAL PROCEDURES

Synthesis details for key compounds. All solvents used were commercially available and were used without further purification. Starting materials used were either available from commercial sources or prepared according to literature procedures.

The ¹H and ¹³C nuclear magnetic resonance (NMR) spectra were recorded on a Bruker 400 at 400 and 100 MHz, or on a Varian Gemini 300 spectrometer operating at 300 and 75 MHz or on a Bruker Avance III 500 spectrometer operating at 500 and 126 MHz, respectively. Spectra were recorded on a NMR spectrometer fitted with a probe of suitable configuration. Spectra were recorded at ambient temperature unless otherwise stated. Chemical shifts are given in ppm down- and upfield from trimethylsilane (TMS) (0.00 ppm). The following reference signals were used: TMS δ 0.00, or the residual solvent signal of DMSO-*d*₆ δ 2.50 (¹H), δ 39.51 (¹³C), CD₃OD δ 3.30 (¹H), δ 49.00 (¹³C), CDCl₃ δ 7.26 (¹H), δ 77.16 (¹³C), CD₃CN δ 1.94 (¹H), δ 118.26 (¹³C), D₂O δ 4.79 (¹H), or TFA δ 11.50 (¹H), δ 164.2 (¹³C), (unless otherwise indicated). Resonance multiplicities are denoted s, d, t, q, m, br, and app for singlet, doublet, triplet, quartet, multiplet, broad, and apparent, respectively.

The analytical purity and the mass spectra (MS) for the test compounds were recorded utilizing thermospray (TS) (Finnigan MAT SSQ 7000, buffer: 50 nM NH₄OAc in CH₃CN:H₂O; 3:7), electron impact (EI) (Finnigan MAT SSQ 710) or electro spray (ES) (LC-MS; LC: Waters 2790, column XTerra MS C₈ 2.5 μ m 2.1 mm \times 30 mm, buffer gradient H₂O + 0.1%TFA:CH₃CN + 0.04%TFA; MS: micromass ZMD) ionization techniques.

Preparative high-performance liquid chromatography (HPLC) was run on a Waters autopurifier HPLC with a diode array detector. Column: Xterra MS C₈, 19 mm \times 300 mm, 10 μ m. Narrow gradients with MeCN/water were used at a flow rate of 20 mL/min.

High resolution mass spectra (HRMS) were recorded on a Micromass Q-ToF (Waters MS Technologies, Manchester, UK) equipped with a LockSpray source and connected to an Acquity ultra performance liquid chromatography (UPLC) system with a photodiode array detectors (PDA) detector (Waters Corp., Milford, USA). All analyses were acquired using positive mode electrospray ionization (ESI+) in full scan, and leucine enkephalin (Sigma) was used as the lock mass (m/z 556.2771) at a concentration of 0.9 pmol/ μ L and a flow rate of 150 μ L/min with a 1:10 split, ion source:waste, or a flow rate of 10 μ L/min. Cone Voltage was set to 54 to achieve approximately 200 counts for leucine enkephalin. Nitrogen was used as the nebulizing and desolvation gas, with the source operated at 120 °C and the desolvation gas at 300 °C. Capillary voltage was 3000 V, cone voltage 30 V, collision energy 5 V. Argon was used as the collision gas. Chromatographic separation was achieved with either a 2.3 min gradient from 5 to 95% acetonitrile (11 mM formic acid, 1 mM NH₄⁺ formate) over an ACQUITY UPLC BEH C18 1.7 μ m, 2.1 mm \times 50 mm column (Waters) maintained at 50 °C and run at a flow rate of 0.85 mL/min with a 1:5 split, ion source:waste, or a 2 min linear gradient from 100% A (A: 10 mM HCOOH) to 100% B (B: MeCN) at a flow rate of 0.4 mL/min with a 1:4 split prior to the ion source. Analytes were diluted in MeOH or DMSO to a suitable concentration for the LC-MS analysis, generally 10 μ M, and 0.1 μ L were injected. Accurate masses of all analytes were obtained from the protonated molecule $[M + H]^+$ and were within 5 ppm mass error (difference between observed protonated mass and calculated protonated mass).

Microwave heating was performed in a Creator or Smith Synthesizer single-mode microwave cavity producing continuous irradiation at 2450 MHz at the indicated temperature in the recommended microwave tubes.

Thin layer chromatography (TLC) was performed on Merck TLC-plates (silica gel 60 F₂₅₄) and UV visualized the spots. Column chromatography was performed using Merck silica gel 60 (0.040–0.063 mm) unless otherwise specified.

The purity of the test compounds was greater than 95% unless specified otherwise.

1-[(4-Bromo-2,5-dimethylphenyl)sulfonyl]-4-methylpiperazine (**6f**). 2-Bromo-1,4-dimethylbenzene, (2.5 g, 13.5 mmol) was cooled to 0 °C, and chlorosulfonic acid (2.2 mL, 33 mmol) was added slowly. The reaction mixture was stirred at 0 °C for 15 min at room temperature for 10 min and subsequently heated at 80 °C for 3 h. The reaction mixture was cooled to room temperature and slowly added to an ice/water mixture. The formed precipitate was dissolved in a mixture of dichloromethane and tetrahydrofuran (10:1) and washed with saturated sodium bicarbonate (aq). The organic phase was dried over sodium sulfate and filtered, and the solvent was removed in vacuo to give 1.3 g of the crude sulfonyl chloride that was dissolved in tetrahydrofuran (20 mL) and cooled to 0 °C. 1-Methylpiperazine (2.5 mL, 22.6 mmol) was added, and stirring was continued for 30 min at room temperature. Saturated sodium hydrogencarbonate (aq 20 mL) was added, and the mixture was extracted with dichloromethane. The combined organic phases were dried over sodium sulfate and filtered, and the solvent was removed in vacuo. The resulting residue was purified by column chromatography using a gradient of methanol in ethyl acetate (0–50%) as the eluent to give 1.50 g (32% yield) of the title compound. ¹H NMR (400 MHz, DMSO-*d*₆) δ 7.71 (m, 2H), 3.02 (m, 4H), 2.48 (s, 3H), 2.37 (s, 3H), 2.32 (m, 4H), 2.14 (s, 3H).

3-Amino-6-[2,5-dimethyl-4-[(4-methylpiperazin-1-yl)sulfonyl]phenyl]-N-pyridin-3-ylpyrazine-2-carboxamide Hydrochloride (**13**). Triisopropylborate (0.40 mL, 1.73 mmol) was added to a solution of 1-[(4-bromo-2,5-dimethylphenyl)sulfonyl]-4-methylpiperazine (**6f**) (0.200 g, 0.58 mmol) in anhydrous tetrahydrofuran (10 mL) at –78 °C under an atmosphere of nitrogen followed by dropwise addition of *n*-butyllithium (1.2 mL, 1.80 mmol, 1.5 M) over 30 min. The resulting mixture was stirred at –78 °C for 1 h, hydrochloric acid (1 M, 1.8 mL, 1.8 mmol) was added, and the reaction mixture was allowed to warm to room temperature. Sodium carbonate (0.382 g, 3.6 mmol) was added, followed by addition of **33** (0.40 g, 0.14 mmol) and Pd(dppf)Cl₂ (40 mg, 0.033 mmol). The resulting mixture was heated at 70 °C overnight. Silica was added, the solvent was evaporated, and the residue was purified by chromatography using a

gradient of ethyl acetate/heptane, (1:100), to ethyl acetate/methanol (10:1). Hydrochloric acid in diethyl ether (1 M, 5 mL) was added to a solution of the base in a mixture of dichloromethane and methanol (3:1, 3 mL). The formed precipitate was collected by filtration, washed with diethyl ether, and dried in vacuo to give 90 mg (48% yield) of the title compound. ¹H NMR (400 MHz, D₂O) δ 9.40 (m, 1H), 8.59 (m, 1H), 8.55 (m, 1H), 8.36 (s, 1H), 8.03 (ddd, *J* = 9, 6, 1 Hz, 1H), 7.78 (s, 1H), 7.50 (s, 1H), 3.90 (d, *J* = 12 Hz, 2H), 3.60 (d, *J* = 11 Hz, 2H), 3.18 (m, 4H), 2.93 (s, 3H), 2.52 (s, 3H), 2.38 (s, 3H).

3-Amino-6-[4-[(2-methoxyethyl)amino]sulfonyl]phenyl]-N-3-pyridinyl-2-pyrazinecarboxamide (**16**). Compound **16** was prepared in 33% yield from 4-bromo-*N*-(2-methoxyethyl)-benzenesulfonamide¹⁷ (**6i**) using a similar procedure to that of **13**. Purification was by column chromatography using dichloromethane/methanol (98:2), followed by a second column chromatography using *n*-heptane/ethyl acetate (1:1) followed by ethyl acetate (100%). ¹H NMR (400 MHz, DMSO-*d*₆) δ 10.61 (s, 1H), 9.03 (s, 1H), 8.99 (d, 1H), 8.42–8.50 (m, 2H), 8.38 (dd, 1H), 8.18–8.26 (m, 1H), 7.88 (d, 2H), 7.75–7.86 (m, 2H), 7.45 (dd, 1H), 3.18 (s, 3H), 2.94 (q, 2H), (2H under the water peak).

3-Amino-6-[4-[(4-methylpiperazin-1-yl)sulfonyl]phenyl]-N-pyridin-3-ylpyrazine-2-carboxamide Hydrochloride (**18**). A suspension of 4-[(4-methylpiperazin-1-yl)sulfonyl]phenylboronic acid¹⁸ (0.199 g, 0.70 mmol), **33** (0.200 g, 0.68 mmol), and Pd(dppf)Cl₂ \times CH₂Cl₂ (0.029 g, 0.036 mmol) in a mixture of toluene (10 mL), ethanol (2 mL), and Na₂CO₃ (2 M, 1 mL) was heated at 80 °C overnight. Silica was added, and the solvent was evaporated. The product was purified by column chromatography using dichloromethane/methanol (93:7) to give 0.244 g (79% yield) of the base as a pale-yellow solid; mp 220–229 °C (decomp). ¹H NMR (400 MHz, DMSO-*d*₆) δ 9.85 (br s, 1H), 8.88 (br s, 1H), 8.75 (s, 1H), 8.45 (d, *J* = 4 Hz, 1H), 8.30 (m, 1H), 8.07 (d, *J* = 8 Hz, 2H), 7.88 (d, *J* = 8 Hz, 2H), 7.37 (dd, *J* = 8, 5 Hz, 1H), 3.37 (m, 4H), 2.92 (m, 4H), 2.56 (m, 3H). Hydrochloric acid in diethyl ether (1 M, 0.81 mL) was added to a solution of 3-amino-6-[4-[(4-methylpiperazin-1-yl)sulfonyl]phenyl]-*N*-pyridin-3-ylpyrazine-2-carboxamide (0.096 g, 0.21 mmol) in a mixture of dichloromethane and methanol (0.95:0.05, 8 mL). The yellow precipitate was removed by filtration, washed with diethyl ether, and dried in vacuo to give the title compound as a yellow solid; mp 217–223 °C (decomp).

3-Amino-6-[4-(morpholin-4-ylsulfonyl)phenyl]-N-(pyridin-3-yl)pyrazine-2-carboxamide (**22**). Compound **22** was prepared in 18% yield from 4-(morpholin-4-ylsulfonyl)phenylboronic acid¹⁸ (**7e**) using a similar procedure to that of **18**. Purification was by column chromatography using dichloromethane/methanol (100:1). HRMS: measured m/z $[M + H]^+$ = 441.1342 (theoretical, 441.1345).

3-Amino-6-[4-[(2-(dimethylamino)ethyl)amino]sulfonyl]phenyl]-N-pyridin-3-ylpyrazine-2-carboxamide hydrochloride (**23**). Compound **23** was prepared in 52% yield from 4-[(2-(dimethylamino)ethyl)sulfamoyl]phenylboronic acid¹⁸ (**7f**) using a similar procedure to that of **18**. ¹H NMR (400 MHz, D₂O) δ 8.90 (s, 1H), 8.25 (m, 2H), 8.08 (s, 1H), 7.66 (m, 1H), 7.56 (d, 2H), 7.31 (d, 2H), 3.07 (m, 8H), 1.11 (t, 6H).

3-Amino-6-[4-[(4-methylpiperazin-1-yl)sulfonyl]phenyl]-N-[4-(pyrrolidin-1-ylmethyl)pyridin-3-yl]pyrazine-2-carboxamide Hydrochloride (**25**). Compound **25** was prepared in 23% yield from 4-[(4-methylpiperazin-1-yl)sulfonyl]phenylboronic acid¹⁸ and **34a** using a similar procedure to that of **18**. Purification was by column chromatography using a gradient of ethyl acetate to ethyl acetate/methanol (1:1). ¹H NMR (400 MHz, D₂O) δ 9.01 (s, 1H), 8.79 (d, *J* = 6 Hz, 1H), 8.75 (m, 1H), 8.15 (m, 3H), 7.83 (d, *J* = 9 Hz, 2H), 4.68 (s, 2H), 3.90 (d, *J* = 14 Hz, 2H), 3.56 (d, *J* = 12 Hz, 2H), 3.39 (m, 4H), 3.20 (t, *J* = 12 Hz, 2H), 2.85 (s, 3H), 2.79 (m, 2H), 2.03 (m, 4H).

tert-Butyl 4-(Pyrrolidin-1-ylmethyl)pyridin-3-ylcarbamate¹⁶ (**31a**). *tert*-Butyl 4-formylpyridin-3-ylcarbamate¹⁹ (1.03 g, 4.64 mmol) was dissolved in 1,2-dichloroethane (20 mL) under an atmosphere of nitrogen. Pyrrolidine (0.41 mL, 4.9 mmol) and acetic acid (0.27 mL, 4.72 mmol) were added, and the reaction mixture was stirred for 1 h. Sodium triacetoxyborohydride (1.27 g, 6 mmol) was added, and stirring was continued for 10 h. Sodium hydroxide (1 M, 5 mL, 5 mmol) was added, and the phases were separated. The aqueous

phase was extracted with dichloromethane, the combined organic phases were dried over sodium sulfate, and the solvent was evaporated. The product was purified by column chromatography using a gradient of methanol in dichloromethane (100:2–100:10) to give 900 mg (70% yield) of the title compound as an oil. ¹H NMR (400 MHz, CDCl₃) δ 9.83 (s, 1H), 9.21 (s, 1H), 8.16 (d, *J* = 5 Hz, 1H), 6.96 (d, *J* = 5 Hz, 1H), 3.66 (s, 2H), 2.49 (m, 4H), 1.81 (m, 4H), 1.52 (s, 9 H).

4-(Pyrrolidin-1-ylmethyl)pyridin-3-amine¹⁶ (**32a**). Trifluoroacetic acid (3 mL, 39 mmol) was added to a stirred solution of **31a** (1.0 g, 3.6 mmol) in dichloromethane (20 mL), and the resulting mixture was stirred for 30 min. The solvent was removed in vacuo. Ethyl acetate (5 mL) was added and removed in vacuo, and this procedure was repeated three times. The residue was dissolved in methanol (50 mL), and DOWEX-OH was added until the methanolic solution was basic. Filtration and removal of the solvent in vacuo gave 0.573 mg (90% yield) of the title compound. ¹H NMR (400 MHz, CD₃OD) δ 7.92 (s, 1H), 7.75 (d, *J* = 5 Hz, 1H), 7.05 (d, *J* = 5 Hz, 1H), 3.61 (s, 2H), 2.49 (m, 4H), 1.79 (m, 4H).

3-Amino-6-bromo-N-pyridin-3-ylpyrazine-2-carboxamide¹⁶ (**33**). Methyl 3-amino-6-bromo-2-pyrazinecarboxylate²⁰ (1.0 g, 4.3 mmol) and 1,8-diazabicyclo[5.4.0]undec-7-ene (645 μL, 4.3 mmol) were added at 70 °C to 3-aminopyridine (10 g, 106 mmol), and the resulting mixture was stirred for 4 h. The reaction mixture was diluted with water (75 mL) and extracted with dichloromethane. The combined organic phases were washed with aqueous saturated ammonium chloride and dried over magnesium sulfate, and the solvent was evaporated in vacuo. The product was purified by column chromatography using dichloromethane/ethanol (9:1) to give 750 mg (59% yield) of the title compound as a yellow solid. ¹H NMR (400 MHz, CDCl₃) δ 9.50 (br s, 1H), 8.82 (d, *J* = 3 Hz, 1H), 8.43 (dd, *J* = 5 and 1 Hz, 1H), 8.31 (s, 1H), 8.23 (ddd, *J* = 8, 3, 2 Hz, 1H), 7.34 (dd, *J* = 8, 5 Hz, 1H).

3-Amino-6-bromo-N-[4-(pyrrolidin-1-ylmethyl)pyridin-3-yl]pyrazine-2-carboxamide¹⁶ (**34a**). 3-Amino-6-bromopyrazine-2-carboxylic acid²⁰ (148 mg, 0.68 mmol), **32a** (100 mg, 0.56 mmol), 2-(1*H*-benzotriazol-1-yl)-1,1,3,3-tetramethyluroniumtetrafluoroborate (288 mg, 0.89 mmol), 1-hydroxybenzotriazole hydrate (118 mg, 0.87 mmol), and *N,N*-diisopropylethylamine (0.2 mL, 1.15 mmol) were suspended in anhydrous acetonitrile (8 mL) and stirred under an atmosphere of nitrogen at room temperature for 12 h. The solvent was removed in vacuo, and the residue was partitioned between dichloromethane and saturated aqueous sodium bicarbonate. The organic phase was dried over sodium sulfate, and the solvent was evaporated in vacuo. The product was purified by column chromatography using a gradient of ethyl acetate in *n*-heptane (1:1–4:1) to give 210 mg (98% yield) of the title compound as a light-brown solid. ¹H NMR (400 MHz, DMSO-*d*₆) δ 11.97 (s, 1H), 9.41 (s, 1H), 8.46 (s, 1H), 8.30 (d, *J* = 5 Hz, 1H), 7.84 (br s, 2H), 7.34 (d, *J* = 5 Hz, 1H), 3.77 (s, 2H), 2.57 (m, 4H), 1.84 (m, 4H).

1-(4-Bromobenzoyl)-4-methylpiperazine¹⁶ (**36a**). 4-Bromobenzoic acid (3.0 g, 14.9 mmol) was dissolved in refluxing thionyl chloride (35 mL), and the solution was heated at reflux for 1 h and then cooled to room temperature. The solvent was evaporated, coevaporated with toluene (3 × 40 mL), and the resulting solid dried in vacuo. The solid was dissolved in dichloromethane (18 mL), cooled in an ice-bath, and 1-methylpiperazine (1.5 mL, 13.6 mmol) added dropwise to give a solid. Dichloromethane and aqueous potassium carbonate were added, and the aqueous phase was extracted with dichloromethane. The combined organic phases were dried over Na₂SO₄ and filtered, and the solvent was evaporated to give 3.86 g (91% yield) of the title compound. ¹H NMR (300 MHz, DMSO-*d*₆) δ 7.64 (d, *J* = 8 Hz, 2H), 7.34 (d, *J* = 8 Hz, 2H), 3.59 (m, 4H), 2.34 (m, 4H), 2.21 (s, 3H).

3-Amino-6-[4-[(4-methylpiperazin-1-yl)carbonyl]phenyl]-N-pyridin-3-ylpyrazine-2-carboxamide Hydrochloride (**37**). Compound **37** was prepared in 26% yield from **36a** using a similar procedure to that of **13**. ¹H NMR (300 MHz, DMSO-*d*₆) δ 11.41 (br s, 1H), 11.11 (s, 1H), 9.40 (s, 1H), 9.06 (s, 1H), 8.90 (d, *J* = 9 Hz, 1H), 8.69 (d, *J* = 5 Hz, 1H), 8.38 (d, *J* = 8 Hz, 2H), 8.06 (dd, *J* = 9, 6 Hz, 1H), 7.59 (d, *J* = 8 Hz, 2H), 3.39 (m, 4H), 3.13 (m, 2H), 2.77 (s, 3H), 2.50 (m, 2H).

3-Amino-6-bromo-N-(3-methoxypropyl)pyrazine-2-carboxamide (**48c**). 3-Methoxy-propylamine (2.1 mL, 20.5 mmol) was added to a mixture of 2-amino-5-bromonicotinic acid (3.0 g, 10.0 mmol), *O*-(benzotriazol-1-yl)-*N,N,N',N'*-tetramethyluronium tetrafluoroborate (4.42 g, 13.8 mmol), 1-hydroxybenzotriazole hydrate (2.54 g, 16.6 mmol), and *N*-ethyl-*N,N*-diisopropylamine (4.8 mL, 27.6 mmol) in anhydrous *N,N*-dimethylformamide (25 mL). The reaction mixture was stirred overnight. The solvent was evaporated, and the product was purified by column chromatography using dichloromethane/methanol (95:5) as the eluent to give a 3.52 g (42% yield) of the title compound. ¹H NMR (400 MHz, DMSO-*d*₆) δ 8.64 (m, 1H), 8.33 (s, 1H), 7.70 (br s, 2H), 3.37 (t, *J* = 6 Hz, 2H), 3.31 (t, *J* = 7 Hz, 2H), 3.24 (s, 3H), 1.75 (quin, *J* = 7 Hz, 2H).

3-Amino-N-(3-methoxypropyl)-6-[4-[(4-methylpiperazin-1-yl)sulfonyl]phenyl]pyrazine-2-carboxamide Hydrochloride (**51**). Compound **51** was prepared as a yellow solid in 19% yield from 1-[(4-bromophenyl)sulfonyl]-4-methylpiperazine²¹ and **48c** using a similar procedure to that of **13**. Purification was by column chromatography using a gradient of dichloromethane/methanol/triethyl amine (9:1:0.1) in methanol (0–100%). ¹H NMR (400 MHz, DMSO-*d*₆) δ 11.02 (br s, 1H), 8.97 (s, 2H), 8.46 (d, *J* = 9 Hz, 2H), 7.82 (d, *J* = 9 Hz, 2H), 3.82 (d, *J* = 13 Hz, 2H), 3.41 (m, 6H), 3.27 (s, 3H), 3.15 (m, 2H), 2.72 (m, 5H), 1.81 (m, 2H).

■ ASSOCIATED CONTENT

● Supporting Information

Synthesis details for nonkey compounds, GSK3β and CDK2 X-ray data collection and refinement statistics, protein expression and purification of GSK3β and CDK2 used for crystallization, crystallization of GSK3β and CDK2, data collection and structure determination. This material is available free of charge via the Internet at <http://pubs.acs.org>.

Accession Codes

PDB ID GSK3β: compound **18**, 4acd; compound **23**, 4acc; compound **25**, 4acg; compound **51**, 4ach. PDB ID CDK2: compound **23**, 4acm.

■ AUTHOR INFORMATION

Corresponding Author

*Phone: +46855326000. E-mail: Stefan.berg@astrazeneca.com.

Notes

The authors declare no competing financial interest.

■ ACKNOWLEDGMENTS

We thank all colleagues in the Department of DMPK AstraZeneca Södertälje who helped to generate the *in vivo* permeability data presented, Fanny Bjarnemark and Ylva Roddis, Department of Medicinal Chemistry, AstraZeneca Södertälje, for generation of HRMS data and Susanne Olofsson and Alexandra Bernlind, Department of Medicinal Chemistry, AstraZeneca Södertälje, for valuable NMR support, I. Janssen, C. Dartsch, and R. Svensson, AstraZeneca Biotech Laboratories, for production of GSK3β protein, Tomas Lundqvist, Department of Structure & Biophysics, AstraZeneca, Mölndal, for his contribution in data collection and initial structure determination of GSK3β complexes, Judith Stanway for expression of CDK2 in baculovirus infected insect cells, Malcolm Anderson for purification of CDK2 protein for crystallization, Claire Brassington for CDK2 crystallization and soaking, and Andrew Pannifer, Helen McMiken, and the staff at the ESRF for assistance with CDK2 X-ray diffraction data collection.

■ ABBREVIATIONS USED

Aβ, β-amyloid; AD, Alzheimer's disease; ATP, adenosine triphosphate; BBB, blood–brain barrier; *n*-BuLi, normal-butyl lithium;

CDK2, cyclin dependent kinase 2; CNS, central nervous system; DIPEA, *N,N*-diisopropylethylamine; DBU, 1,8-diazabicyclo[5.4.0]-undec-7-ene; DCM, dichloromethane; DIPC, *N,N'*-diisopropylcarbodiimide; DMAP, dimethylaminopyridine; DME, 1,2-dimethoxy-methane; DMF, *N,N*-dimethylformamide; DMSO, dimethyl sulfoxide; DTT, dithiothreitol; EDCl, 1-ethyl-3-(3-dimethyl-aminopropyl)carbodiimide; EDTA, ethylenediaminetetraacetic acid; EI, electron Impact; ES, electro spray; ESI, electro spray ionization; GSK3 β , glycogen synthase kinase-3 β ; HEPES, 4-(2-hydroxyethyl)-1-piperazinesulfonic acid; HTS, high throughput screening; HOBT, 1-hydroxybenzotriazole; HPLC, high performance liquid chromatography; HRMS, high resolution mass spectra; LC, liquid chromatography; MS, mass spectra; MOPS, morpholinopropanesulfonic acid; NFTs, neurofibrillary tangles; NMO, *N*-methylmorpholine-*N*-oxide; NMR, nuclear magnetic resonance; MW, microwave; PDA, photodiode array detectors; PHFs, paired helical filaments; PyBroP, bromo-tris-pyrrolidino phosphoniumhexafluorophosphate; SEM, standard error of the mean; TBTU, *O*-(benzotriazol-1-yl)-*N,N,N',N'*-tetramethyluronium tetrafluoroborate; TFA, trifluoroacetic acid; THF, tetrahydrofuran; TMS, trimethylsilane; TS, thermospray; UPLC, ultra performance liquid chromatography

■ REFERENCES

- (1) Alzheimer, A. Über eigenartige krankheitsfälle des späteren alters. *Z. Gesamte Neurol. Psychiatr.* **1911**, *4*, 356–385.
- (2) Yankner, B. A. Mechanisms of neuronal degeneration in Alzheimer's disease. *Neuron* **1996**, *16*, 921–932.
- (3) Pei, J. J.; Braak, H.; Grundke-Iqbal, I.; Winblad, B.; Cowburn, R. F. Distribution of active glycogen synthase kinase 3 β (GSK-3 β) in brains staged for Alzheimer's disease neurofibrillary changes. *J. Neuropathol. Exp. Neurol.* **1999**, *58* (9), 1010–1019.
- (4) Leroy, K.; Boutajangout, A.; Authélet, M.; Woodget, J. R.; Anderton, B. H.; Brion, J.-P. The active form of glycogen synthase kinase-3 β is associated with granulovacuolar degeneration in neurons in Alzheimer's disease. *Acta Neuropathol.* **2002**, *103*, 91–99.
- (5) Bhat, R. V.; Budd Haerberlein, S. L.; Avila, J. Glycogen synthase kinase 3: a drug target for CNS therapies. *J. Neurochem.* **2004**, *89*, 1313–1317.
- (6) Lucas, J. J.; Hernandez, F.; Gomez-Ramos, P.; Moran, M. A.; Hen, R.; Avila, J. Decreased nuclear beta-catenin, tau hyperphosphorylation and neurodegeneration on GSK3 β conditional transgenic mice. *EMBO J.* **2001**, *20*, 27–39.
- (7) Kypka, R. M. Review: GSK3 inhibitors and their potential in the treatment of Alzheimer's disease. *Expert Opin. Ther. Pat.* **2005**, *15* (10), 1315–1331.
- (8) Schultz, C.; Link, A.; Leost, M.; Zaharevitz, D. E.; Gussio, R.; Sausville, E. A.; Meijer, L.; Kunick, C. Paullones, a Series of Cyclin-Dependent Kinase Inhibitors: Synthesis, Evaluation of CDK1/Cyclin B Inhibition, and in Vitro Antitumor Activity. *J. Med. Chem.* **1999**, *42*, 2909–2919.
- (9) Leost, M.; Schultz, C.; Link, A.; Wu, Y.-Z.; Biernat, J.; Mandelkow, E.-M.; Bibb, J. A.; Snyder, G. L.; Greengard, P.; Zaharevitz, D. W.; Gussio, R.; Senderowicz, A. M.; Sausville, E. A.; Kunick, C.; Meijer, L. Paullones are potent inhibitors of glycogen synthase kinase-3 β and cyclin-dependent kinase 5/p25. *Eur. J. Biochem.* **2000**, *267*, 5983–5994.
- (10) Coghlan, M. P.; Culbert, A. A.; Cross, D. A. E.; Corcoran, S. L.; Yates, J. W.; Pearce, N. J.; Rausch, O. L.; Murphy, G. J.; Carter, P. S.; Cox, L. R.; Mills, D.; Brown, M. J.; Haigh, D.; Ward, R. W.; Smith, D. G.; Murray, K. J.; Reith, A. D.; Holder, J. C. Selective small molecule inhibitors of glycogen synthase kinase-3 modulate glycogen metabolism and gene transcription. *Chem. Biol.* **2000**, *7* (9), 793–803.
- (11) Bhat, R.; Xue, Y.; Berg, S.; Hellberg, S.; Ormö, M.; Nilsson, Y.; Radesäter, A.-C.; Jerning, E.; Markgren, P.-O.; Borgegård, T.; Nylöf, M.; Giménez-Cassina, A.; Hernández, F.; Lucas, J. J.; Diaz-Nido, J.; Avila, J. Structural insights and biological effects of glycogen synthase kinase 3-specific inhibitor AR-A014418. *J. Biol. Chem.* **2003**, *46* (278), 45937–45945.
- (12) Uno, Y.; Iwashita, H.; Tsukamoto, T.; Uchiyama, N.; Kawamoto, T.; Kori, M.; Nakanishi, A. Efficacy of a novel, orally active GSK-3 inhibitor 6-methyl-*N*-[3-[[3-(1-methylethoxy)propyl]-carbamoyl]-1*H*-pyrazol-4-yl]pyridine-3-carboxamide in tau transgenic mice. *Brain Res.* **2009**, *1296*, 148–163.
- (13) Ellingson, R. C.; Henry, R. L. Pyrazine Chemistry. IV. Bromination of 2-Amino-3-carbomethoxy-pyrazine. *J. Am. Chem. Soc.* **1949**, *71* (8), 2798–2800.
- (14) Zhang, N.; Zhong, R.; Yan, H.; Jiang, Y. Structural Features Underlying Selective Inhibition of GSK3 β by Dibromocantharelline: Implications for Rational Drug Design. *Chem. Biol. Drug. Des.* **2011**, *77*, 199–205.
- (15) Cecchelli, R.; Dehouck, B.; Descamps, L.; Fenart, L.; Buee-Scherrer, V.; Duhem, C.; Lundquist, S.; Rentfel, M.; Torpier, G.; Dehouck, M. P. In vitro model for evaluating drug transport across the blood-brain barrier. *Adv. Drug Delivery Rev.* **1999**, *5*, 165–178.
- (16) Berg, S.; Hellberg Arylamines for the treatment of conditions associated with GSK-3. PCT Int. Appl. WO 2003004472 A1 20030116, 2003.
- (17) Gatti McArthur, S.; Goetschi, E.; Palmer, W. S., Preparation of acetylenyl-pyrazolo-pyrimidine derivatives for use as mglur2 antagonists treating CNS disorders, PCT Int. Appl. WO 2006099972 A1 20060928, 2006.
- (18) Richardson, C. M.; Nunns, C. L.; Williamson, D. S.; Parratt, M. J.; Dokurno, P.; Howes, R.; Borgognoni, J.; Drysdale, M. J.; Finch, H.; Hubbard, R. E.; Jackson, P. S.; Kierstan, P.; Lentzen, G.; Moore, J. D.; Murray, J. B.; Simmonite, H.; Surgenor, A. E.; Torrance, C. J. Discovery of a potent CDK2 inhibitor with a novel binding mode, using virtual screening and initial, structure-guided lead scoping. *Bioorg. Med. Chem. Lett.* **2007**, *17* (14), 3880–3885.
- (19) Venuti, M. C.; Stephenson, R. A.; Alvarez, R.; Bruno, J. J.; Strosberg, A. M. Inhibitors of cyclic AMP phosphodiesterase. 3. Synthesis and biological evaluation of pyrido and imidazolyl analogs of 1,2,3,5-tetrahydro-2-oxoimidazo[2,1-*b*]quinazoline. *J. Med. Chem.* **1988**, *31*, 2136–2145.
- (20) Ellingson, R. C.; Henry, R. L. Pyrazine Chemistry. IV. Bromination of 2-Amino-3-carbomethoxy-pyrazine. *J. Am. Chem. Soc.* **1949**, *71* (8), 2798–2800.
- (21) Stauffer, S. R.; Huang, Y. R.; Aron, Z. D.; Coletta, C. J.; Sun, J.; Katzenellenbogen, B. S.; Katzenellenbogen, J. A. Triarylpyrazoles with basic side chains: development of pyrazole-based estrogen receptor antagonists. *Bioorg. Med. Chem.* **2001**, *9*, 151–162.